Author/s:
Shi, S;Lam, N;Cui, Y;Lu, G;Gad, E;Zhang, L

Title:
Life-cycle performance of aluminium cladding panels in resisting hailstorms

Date:
2024-05

Citation:
Shi, S., Lam, N., Cui, Y., Lu, G., Gad, E. & Zhang, L. (2024). Life-cycle performance of aluminium cladding panels in resisting hailstorms. Structural Safety, 108, https://doi.org/10.1016/j.strusafe.2024.102439.

Persistent Link:
https://hdl.handle.net/11343/340262

Structural Safety 108 (2024) 102439

Contents lists available at ScienceDirect

Structural Safety

journal homepage: www.elsevier.com/locate/strusafe

Life-cycle performance of aluminium cladding panels in resisting hailstorms

Shuangmin Shi [a], Nelson Lam [a], Yiwen Cui [a], Guoxing Lu [b], Emad Gad [b], Lihai Zhang [a,*]

[a] Department of Infrastructure Engineering, The University of Melbourne, Parkville, VIC, 3010, Australia
[b] School of Engineering, Swinburne University of Technology, Hawthorn, VIC, 3122, Australia

ARTICLE INFO

Keywords:
Life-cycle performance
Hail size distribution
Repeated impact
Permanent indentation
Stochastic model

ABSTRACT

This paper delves into cumulative damage on aluminium cladding panels attributed to hailstorms throughout the lifespan of the installations. 40 gas gun tests subjecting the cladding panel to repeated impact were undertaken for the purpose of studying cumulative damage behaviour. Insights from these tests were integrated into a hail size distribution model to characterise the probabilistic distribution of permanent indentation resulted from multiple hailstorm events. A life-cycle analysis framework was subsequently introduced, incorporating the natural variability of hailstone sizes and dynamic response of claddings to repeated ice impact. Intervention criterion can be established based on knowledge of the accumulation of permanent indentation into the cladding panels. Proactive actions are recommended should the indentations become visible to prevent worsening damage. Randomness of hailstorm occurrences was considered using hazard function which can be inferred from historical observations. Practical application of the proposed model is illustrated through case studies of two Australian states, coupled with comparative analyses highlighting key factors influencing cladding performance. The ability to account for stochasticity distinguishes the presented framework from existing deterministic approaches.

1. Introduction

Claddings in a building are highly susceptible to damage caused by extreme weather such as hailstorms. Impact by hailstones can deface the surface of the cladding panel, necessitating replacement. In more severe cases, the intensity of the impact can be high enough to perforate the cladding, allowing the ingress of water to occur. Damage caused to the interior of a building can be extensive as a result. Tens of millions of dollars may be allocated to attending to damage and disruption caused to a building in a major hailstorm, and to mitigate risks in the future [1–3]. A reliable methodology for predicting the extent of damage to claddings and for assessing performance over the entire lifespan of the building is warranted. Building designers and operator are then empowered to make well-informed decisions based on realistic risk assessments, and to effectively implement the optimisation of preventive measures.

The impact action of flying projectiles onto the claddings is considerably more intricate compared to collision by a heavy moving object on a structural member [4–7]. In the scenario of a floor beam experiencing impact by a heavy fallen object, for example, deformation caused to the beam would primarily be associated with global impulsive actions that can be modelled using equal momentum and energy principles [8]. Modelling techniques have been developed to predict contact force generated by the impact [9–12]. Modelling impact by windborne debris and hail, and the resulting damage to claddings and facades presents a much greater challenge [13–19]. The rapid disintegration of a hailstone on impact with the surface of the target adds to the complexity. Extensive experimental investigations [20,21], analytical studies [22–24], and numerical simulations [25–28] have been conducted to examine contact force that is generated by hail on a metal, or glazing, surface.

Investigation into hail-induced damage on metal claddings, or glazing panels, have been based on deterministic modelling which aims at making predictions of the outcome of a predetermined impact scenario expressed in terms of the size of the hailstone and the velocity of impact. Predictions based on the most onerous (deterministic) scenario, forming part of the design process, do not account for variability in the size of individual hailstones in a real storm. Overly conservative design outcomes can be transpired from these methods of predictions. Incorporating the distribution of the size of hailstones offers insights into the performance of claddings spanning the service life of a building.

* Corresponding author.
E-mail addresses: shuangmin@unimelb.edu.au (S. Shi), ntkl@unimelb.edu.au (N. Lam), yiwcui1@student.unimelb.edu.au (Y. Cui), glu@swin.edu.au (G. Lu), egad@swin.edu.au (E. Gad), lihzhang@unimelb.edu.au (L. Zhang).

https://doi.org/10.1016/j.strusafe.2024.102439
Received 15 September 2023; Received in revised form 25 October 2023; Accepted 15 January 2024
Available online 18 January 2024

Empirical studies have been undertaken to examine the effects of the size, and the (randomised) shape, of hailstones on the peak contact force [29]. The spatial distribution of Griffth flaws in glazing panels has also been randomised for modelling the probability of fracture in glass [30,31]. However, no report on similar studies on damage to metal claddings adopting the probabilistic approach to take into account variabilities of the various parameters controlling the damage outcome can be found in the literature.

Claddings in a building are expected to provide robust resistance to severe weather conditions including hailstorms. Testing protocols stipulated by national standards which are concerned with hail resistance of claddings are typically about certification of products based on pass/fail outcome of prescribed testings (e.g., ANSI/FM_4473, AS/NZS 1170.2). Claddings once installed in exposed locations become vulnerable to structural impairments which is accumulative in nature when subjected to repeated strikes by debris, and hail, in multiple storm events during the service life of the installation. This incremental deterioration poses a considerable risk to the service life of the cladding. Research has been conducted to model progressive degradation of a structure using time-dependent reliability analysis [32–35]. This modelling approach offers a comprehensive life-cycle perspective of system performance [36–38], and has demonstrated its versatility across a diversity of engineering applications, including the evaluation of concrete resistance to corrosion [39–42], damage caused to bridges in earthquakes [43], and the adverse effects of natural disasters on a waste management system [44,45]. When evaluating the life-cycle performance of claddings, reliability analysis can be adapted for predicting the expected lifespan of claddings and the required rate of intervention taking into account behavioural phenomena in a hailstorm and physical properties of the claddings.

In this study, investigation into the probabilistic distribution of the size of hail in a storm and the resulting permanent indentation into aluminium alloy cladding was first conducted. An experimental program involving 40 gas gun propelled impact tests on cladding specimens was performed in support of the model development. An important original contribution of this study is the introduction of a reliability-based framework for predicting damage caused to claddings that are exposed to hail hazard, along with the probability of intervention that is required throughout the lifespan of the building. To achieve realistic estimation, the proposed methodology employs a *marked point process* approach which integrates uncertainties associated with hailstorm intensity and the rate of occurrence as illustrated in the schematic diagram of Fig. 1. The concept of *marked point process* has been utilised to model failure and deterioration of structures over time [46–49], where points indicate the occurrence of the events (e.g., $T_1, T_2, \cdots$ in Fig. 1) and marks associated with each event represent the severity of the damage (e.g., $W_1, W_2, \cdots$ in Fig. 1). The key components of this study are presented in the form of a flow chart (Fig. 2). The highlight of the proposed framework lies in its integration of hail particle size distribution and insights from gas gun testing, which facilitates a more faithful modelling of the performance of claddings when subjected to multiple hail impact. The introduction of hail particle size distribution enables the damage potential on the panel to be characterised probabilistically, accounting for the natural variations in the size of individual hailstones. The proposed framework is anticipated to provide more realistic predictions than that obtained from currently known methods. Designers, stakeholders, and policy makers, will then be enabled to make well-informed decisions as a result. The remainder of this paper is structured as follows:

I. Experimental investigation of the accumulation of indentation into the surface of the cladding when subjected to repeated strikes by hail (Section 2)
II. Modelling the distribution of indentation taking into account the size distribution of hail in a storm (Section 3)
III. Development of the key parameters in the life-cycle analysis framework (Section 4)
IV. Presentation of 2 case studies based at the Australian state of Victoria and New South Wales, to illustrate the application of the proposed methodology (Section 5)

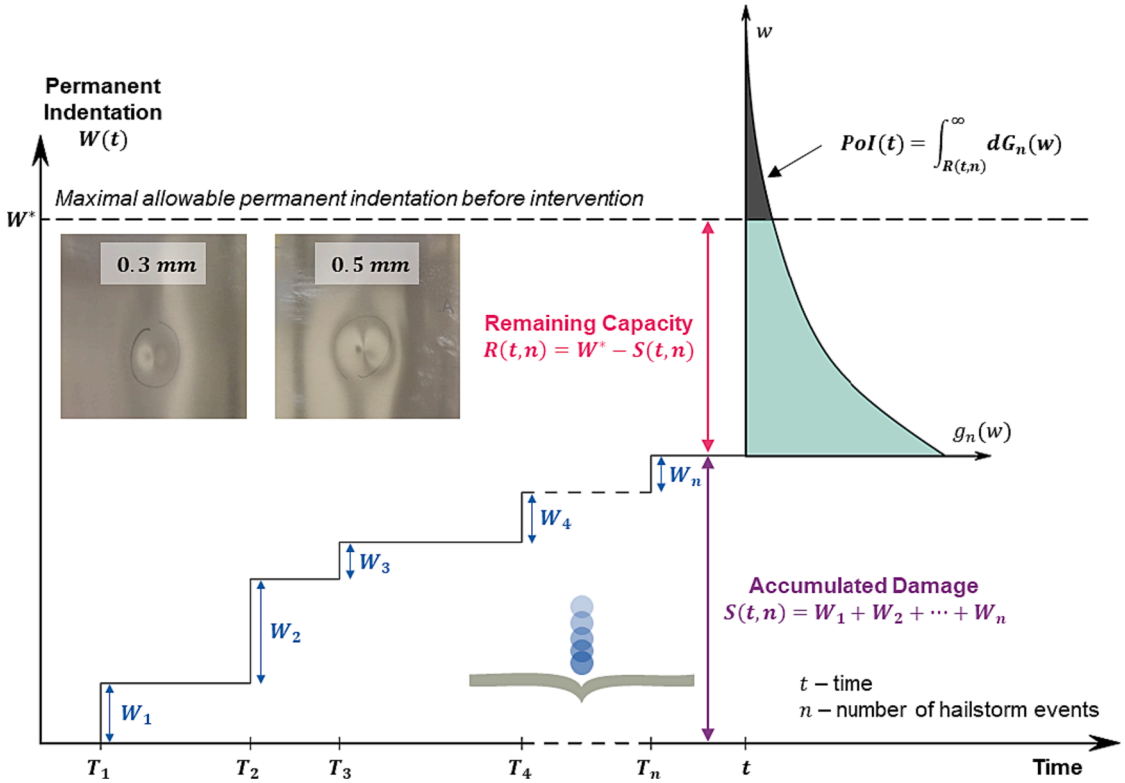

Fig. 1. Conceptual diagram and definition of the terminologies used in computing the probability of intervention after n hailstorm events.

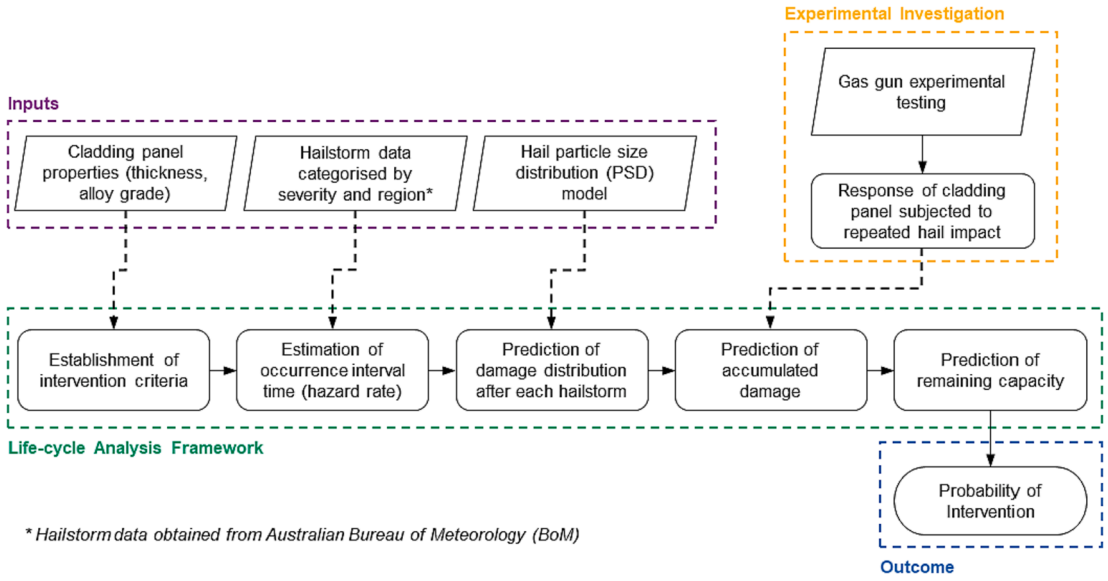

Fig. 2. A flowchart overview of the proposed life-cycle analysis framework in this study.

2. Damage accumulation of cladding panels subjected to repeated hail impact

2.1. Experiment setup

Ice spheres fabricated using a custom-designed mould [24] was used as impactor in the impact tests to mimic real hailstones. The top-down freezing method for making ice spheres as introduced in the previous work [20,24] serves the purpose of eliminating air voids that could otherwise alter the strength, and stiffness, of the impactor. This method of preparing ice specimens was aimed at ensuring the replicability of measurements taken from predetermined impact scenarios, thereby facilitating like-with-like comparison across studies. It is acknowledged that natural hailstones typically contain trapped air bubbles during their formation process within the cloud. Thus impact by an ice specimen that was prepared by the method employed in this study is expected to result in a higher intensity impact action than a naturally occurring hailstone of the same size and impact velocity. The chosen diameter of the ice sphere was 50.8 mm (2 in.) which was consistent with the upper limit stipulated by the well-known regulatory document (ANSI/FM_4473 2011) for the impact testing of roof panels for hail resistance. It is recognised that natural hailstones are irregular in shape unlike ice impactors employed in the study. Nonetheless, an investigation reported in the literature made the observation that the amount of contact force generated by a spherical impactor was consistent with the median of the probabilistic distribution of contact forces generated by irregularly shaped impactors for a fixed mass of the impactor and the velocity of impact [29].

Aluminium panels with gross dimensions: (1) 900 mm x 900 mm x 3 mm thick and (2) 900 mm x 900 mm x 4 mm thick, were employed as the test specimens. The choice of the panel thickness was consistent with that of common alloy cladding products in the global market. Claddings of thickness exceeding 4 mm can be found with aluminium composite panels (featuring a honeycomb core), but rarely with alloy panels. Cladding with thickness below 3 mm were not included into the experimental programs, as those products are typically not favoured by building owners, and designers, to be used in exposed locations because of the likelihood of widespread damage sustained in a severe storm. The planar dimensions of the panel, and the location of impact, have been shown to have negligible influence on the amount of permanent indentation and flexural strain resulted from ice impact [18,50]. The alloy grade for the test specimens was 5083-H116. The material properties are summarised in Table 1.

The experimental setup, as shown diagrammatically in Fig. 3a, and by the photos shown in Fig. 3b, featured the use of compressed nitrogen gas to propel an ice sphere in a guiding tube targeting at the aluminium test specimen which was supported by a custom-designed steel frame (built of 10 mm thick steel sections assembled by bolts) which had the panel fully clamped at all the edges. To suppress any melting of the ice impactor during launching, the guiding tube was made of PVC with low thermal conductivity. The impact velocity of the ice projectile was measured using a high-speed camera (*Phantom V2512*) which was positioned close to the frontal surface of the panel. The shooting angle was at 90 degrees to the projectile trajectory for achieving better accuracy with measurements taken from the impact tests. The high-speed camera captured images at a rate of 86,000 frames per second. In parallel with high-speed photogrammetry, a laser sensor (*Micro-Epsilon optoNCDT-2300*) was firmly attached to a stationary steel I-beam at the rear side of the panel to capture the displacement time history at the position of impact. Displacement measurements acquired from the laser sensor were sampled at a frequency of 20 kHz with the use of an oscilloscope (*Tektronix TBS 2000B*). The laser sensor was set with an edge falling slope trigger mode, and was synchronised with the high-speed camera to accurately match the captured images of the impactor and target with details of their motion. Following testing of the specimen, an optical 3D scanner (*Artec Spider 3D*) was used to survey damage through mapping of the profile of the permanent indentation caused by the impact.

2.2. Results and discussions

In the impact tests, the same test specimen was struck repeatedly at the same position five times by a spherical ice impactor of the same diameter, mass and velocity (within ± 5 % differences). The profile of the dented surface was scanned after each strike by an optical 3D scanner to observe changes to the indentation following each strike. A

Table 1
Material properties of target aluminium panels samples with 3 mm and 4 mm thickness, respectively (ASTM B928M).

Alloy grade	Density (kg/m^3)	Elastic Modulus (*GPa*)	Yield Strength (*MPa*)
5083-H116	2660	71	215

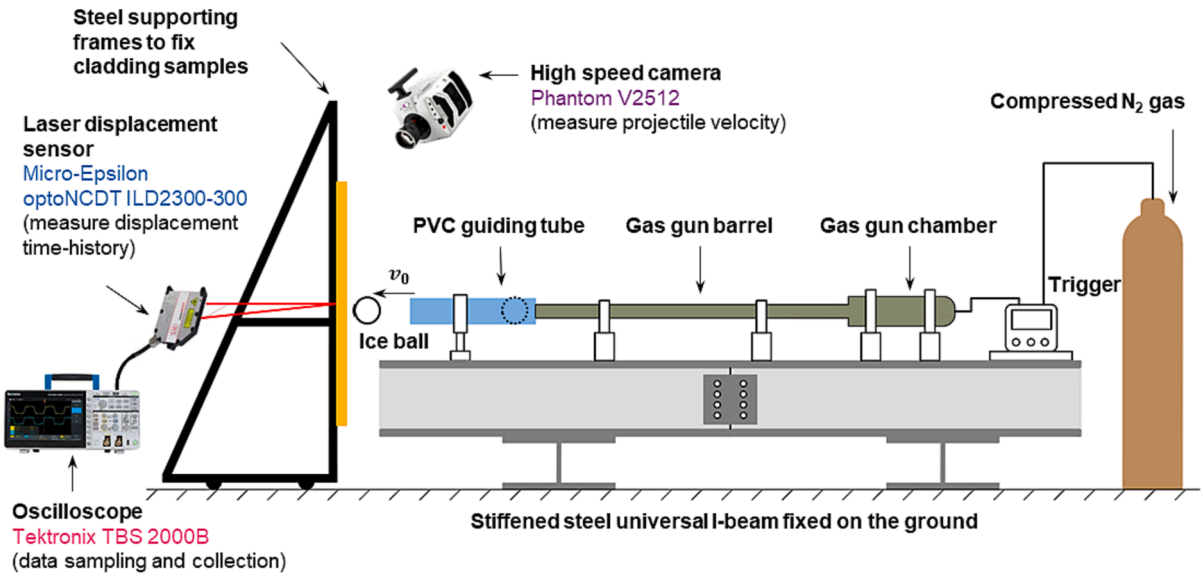

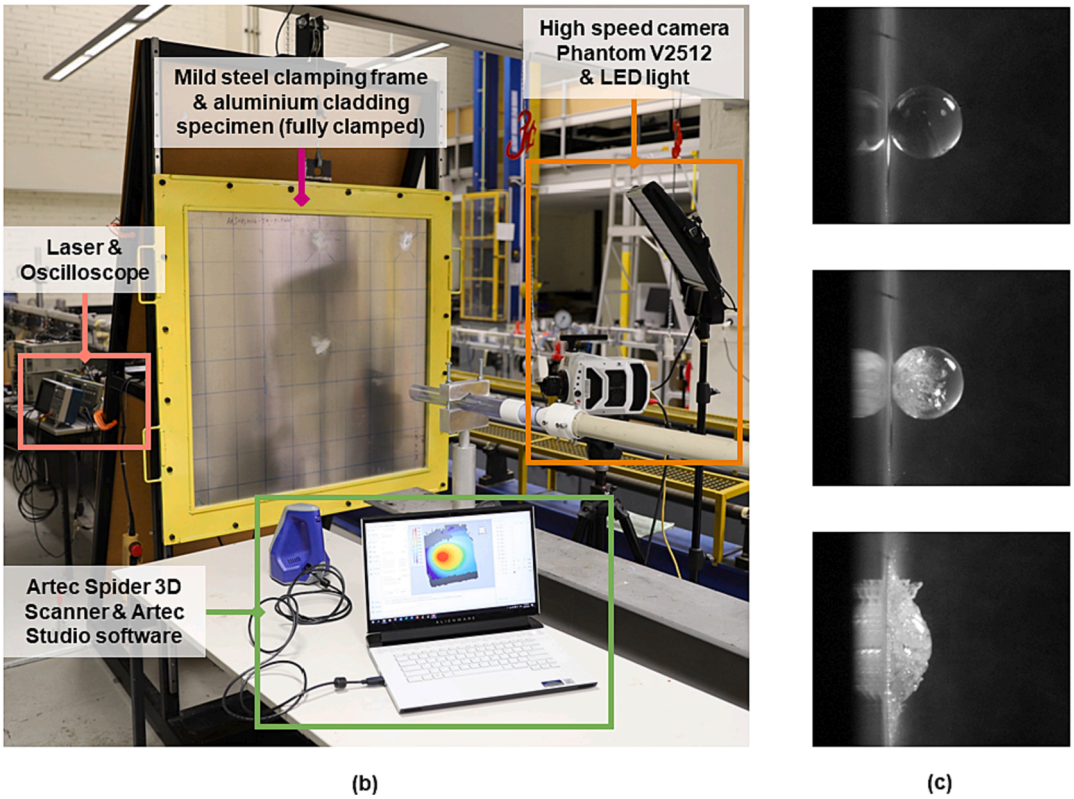

Fig. 3. (a) A schematic diagram of the experimental apparatus used in the impact test (b) photo of the experimental setup (c) images captured by high-speed camera showing the disintegration of ice ball during the impact process.

sample of the measured results taken from two sets of tests are plotted on Fig. 4a and Fig. 4b to illustrate the stepwise change in the permanent indentation profile resulted from repetitive striking.

It is shown in the presented profiles of the permanent indentation that the first strike caused the maximum amount of denting. The second strike caused a significantly lesser amount of increase in denting. The increase was even less with the third strike. After subjecting the same position to three strikes, the increase became negligible with further strikes as the profile became stabilised. The same trend was observed across many sets of tests to cover a range of impact scenarios (of varying panel thickness and impact velocity) as shown in Fig. 5a which presents the correlation of the amount of permanent cumulative indentation at the centre point of impact. Results showing the increase in the permanent indentation, elastic indentation, and the sum of the two (total) indentation recorded from each strike are presented in Fig. 5b in the form of a column bar chart for one set of tests ($h = 3$ mm, $v_0 = 55$ m/s). In summary, a progressive decrease in the increment of the permanent indentation (and stabilisation following the third strike) was observed. Another trend revealed from the test program was the gradual decrease in the amount of elastic deformation, and an increase in the proportion

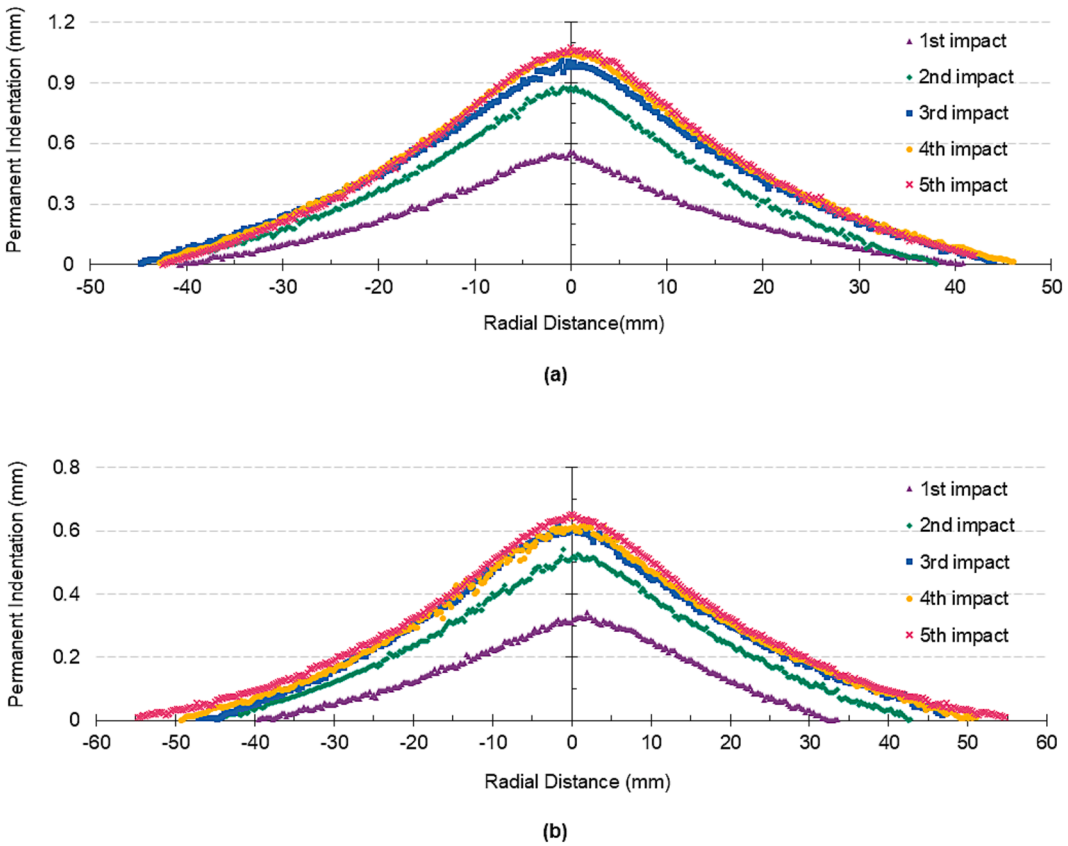

Fig. 4. Indentation profile measured experimentally under repeated impact (a) diameter of ice ball = 50.8 mm, impact velocity ≈ 50 m/s, thickness of panel = 3 mm (b) diameter of ice ball = 50.8 mm, impact velocity ≈ 75 m/s, thickness of panel = 4 mm.

of deformation recovery, with repeated striking.

The amount of plastic energy (W_P) absorbed by a fully clamped aluminium thin plate, which undergoes finite permanent indentation, can be expressed as the summation of the following energy components (i) energy absorbed by radial membrane stresses (W_m), (ii) energy absorbed by bending moments in the radial direction (W_{rb}), and (iii) energy absorbed by bending moments in the circumferential direction ($W_{\theta b}$). Eq. (1) showing the summation is presented along with Eq. (2a) – (2c) to give details of the individual energy terms.

$$W_P = W_m + W_{rb} + W_{\theta b} \tag{1}$$

$$W_m = \pi\sigma_d h \int_0^R \left(\frac{\partial w}{\partial r}\right)^2 r dr \tag{2a}$$

$$W_{rb} = \frac{1}{2}\pi\sigma_d h^2 \int_0^R \left(-\frac{\partial^2 w}{\partial r^2} r\right) dr \tag{2b}$$

$$W_{\theta b} = \frac{1}{2}\pi\sigma_d h^2 \int_0^R \left(-\frac{\partial w}{\partial r}\right) dr \tag{2c}$$

where, h is thickness of the cladding, R is radial distance measured from the point of impact to the edge of the dented area (which can be taken as 50 mm for conservative approximation based on experimental observations); σ_d is dynamic flow stress (as defined by the Cowper-Symonds equation) which is approximately 1.4 times higher than the static yield stress for aluminium alloy materials [50]; w is indentation profile measured from experiments by the use of the optical 3D scanner similar to the examples presented in Fig. 4.

The amount of plastic energy absorbed by the dented panel (W_p) expressed as a fraction of the initial kinetic energy delivered by the impact (referred hereafter as energy ratio) is presented in Fig. 6 across all the test sets covered by the experimental program. The energy ratios associated with the first impact on panels with thickness of 3 mm and 4 mm were approximately 6.5 % and 2.1 %, respectively. The trend of smaller ratios with a thicker panel as observed from the tests were consistent with findings reported in an earlier study based on single strike by hail on the cladding [50]. It is evident that the amount of energy absorbed by the cladding in the form of permanent indentation is gradually decreasing with increasing number of repeated strikes which are targeted at the same position on the cladding. Thus, the degree of damage sustained by the cladding following repeated strikes would stabilise.

The amount of permanent indentation expected after a single hail impact can be estimated using Eq. (3), which was derived by substituting Eqs. (2a) – (2c) into Eq. (1) and then rearranged to solve for the indentation (w_0). The accuracy of Eq. (3) has been proven to be within 8 % from experimental measurements for single impact [50].

$$w_0 = \frac{1}{2}\left(-h\frac{\mathrm{A}}{\mathrm{B}} + \sqrt{h^2\frac{\mathrm{A}^2}{\mathrm{B}^2} + \frac{4W_P}{\pi h\sigma_d \mathrm{A}}}\right) \tag{3}$$

where coefficients A and B are the lower incomplete gamma functions resulted from solving for the integrals of Eqs. (2a) – (2c). The numerical value of B may be taken as 0.94 and 0.77 for panel thickness of 3 mm and 4 mm, respectively; whereas A may be taken as 0.35 irrespective of the panel thickness.

Eq. (3) only provides estimate of the amount of indentation into the aluminium alloy cladding when subjected to the initial strike by an ice sphere. Damage caused to the cladding by multiple strikes is not modelled. As the initially damaged panel is subjected to the repeated strike by the second, and third, ice sphere of identical mass and velocity, the amount of permanent indentation would increase gradually and

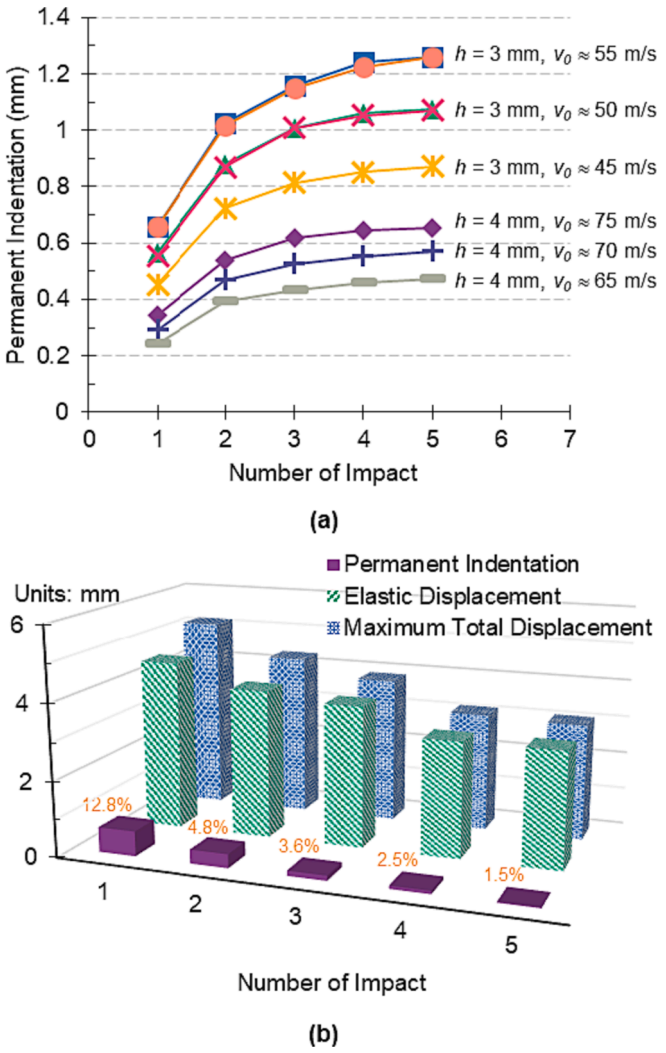

Fig. 5. (a) Permanent indentation measured at the impact point after each ice ball impact across different combinations of impact velocity and panel thickness (b) experimental measurements of increment in permanent indentation, elastic displacement, and maximum total displacement at the impact point for the test group with an ice ball diameter of 50.8 mm, impact velocity of ~ 55 m/s, and panel thickness of 3 mm.

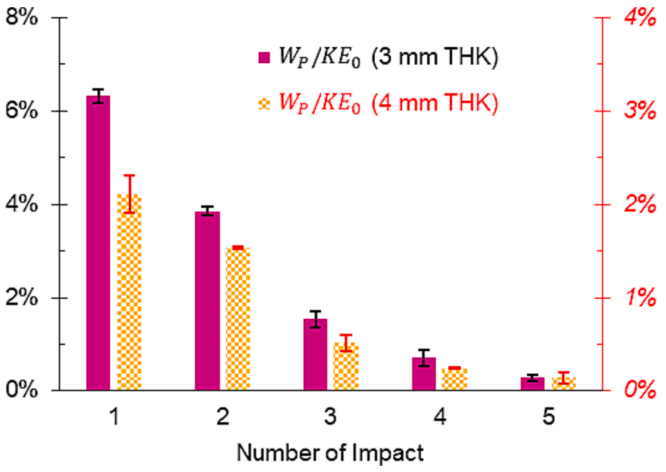

Fig. 6. Plastic energy (W_p) to initial kinetic energy (KE_0) ratios against the number of impacts.

eventually cease to increase by any significant amount when deformation becomes stabilised. Analogous phenomenon has likewise been documented within other engineering scenarios. These observations were initially reported from the slamming of a vessel on a marine structure [51], subsequently evolving to encapsulate the response of a structure under repeated pounding by a rigid object [52,53]. More recently, Eq. (4) which is based on comparing the energy of absorption with the kinetic energy delivered by the impact of a rigid object was established to determine if the response of the structure will stabilise [54,55].

$$E^I_{k0} \le E^P_{me} \tag{4}$$

where E^I_{k0} is the initial kinetic energy delivered by the impactor and E^P_{me} is the maximum amount of elastic strain energy that can be absorbed by the deformed panel. As impact with a similar intensity is repeated on the target, the elastic strain energy absorption capacity would increase with the number of impacts. This increase is the result of the expansion of the elastic limit resulted from modifications caused to the geometry of the target. In situations where the amount of kinetic energy delivered by the impactor is relatively small, Eq. (4) is likely to be satisfied implying the convergence of the plastic deformation. In dealing with impact by ice, Eq. (4) would need to be modified into Eq. (5) which has incorporated an extra term to take into account energy expanded in disintegration of the ice impactor.

$$E^I_{k0} \le E^P_{me} + E^I_d \tag{5}$$

where E^I_d is the energy dissipated by the disintegration of the ice sphere upon impact. The extra term in Eq. (5) means that the criterion is even more likely to be satisfied with an impactor (like an ice sphere) which disintegrates on impact. Upon reaching this state, the targeted panel would not be having any remaining energy absorption capacity. In this state, as deformation becomes stabilised, no further plastic deformation can be caused to the panel when impacted upon repetitively. This phenomenon is evident in observations presented in Fig. 5a.

The amount of permanent indentation caused to aluminium cladding when subjected to repeated strikes by ice can be expressed in Eq. (6) by expanding Eq. (3) in a series form.

$$\begin{aligned} w_{0,i=n} &= \sum_{i=1}^{n} \frac{1}{2}\left(-h\frac{\mathrm{A}}{\mathrm{B}} + \sqrt{h^2\frac{\mathrm{A}^2}{\mathrm{B}^2} + \frac{4W_{P,i=n}}{\pi h\sigma_d \mathrm{A}}} \right) \\ &= -\frac{nh\mathrm{A}}{2\mathrm{B}} + \sum_{i=1}^{n}\sqrt{h^2\frac{\mathrm{A}^2}{\mathrm{B}^2} + \frac{4W_{P,i=n}}{\pi h\sigma_d \mathrm{A}}} \end{aligned} \tag{6}$$

where, n is the number of impacts that a panel is expected to sustain; $w_{0,i=n}$ and $W_{P,i=n}$ are the cumulative permanent indentation at the point of impact and the amount of energy expended in plastic work following the n^{th} impact, respectively. Eq. (6) can be reduced into a more simplified form as shown by Eq. (7) known as the *Hill Function* [56], which is very effective in modelling deformation phenomenon associated with damage to cladding (by hail) [24],concrete [41,57–60], and human biological tissues [61,62].

$$w_{0,i=n} = w_{0,i=1}\beta\left(\frac{n^N}{K^N + n^N}\right) = 2w_{0,i=1}\left(\frac{n^2}{1+n^2}\right) \tag{7}$$

where, β is a multiplier and $w_{0,i=1}\beta$ is the maximum possible cumulative indentation (after the permanent indentation stabilises); K is the number of impacts required to achieve 50 % of the maximum possible cumulative indentation; and N is used to characterise the rate of damage accumulation. It can be shown that if β, K and N of Eq. (7) take the value of 2, 1, and 2, respectively, the predicted amount of indentation from multiple strikes is in very good agreement with experimental measurements (as shown by Fig. 7). The rule-of-the-thumb inferred from the predictions is that the maximum possible cumulative indentation of the

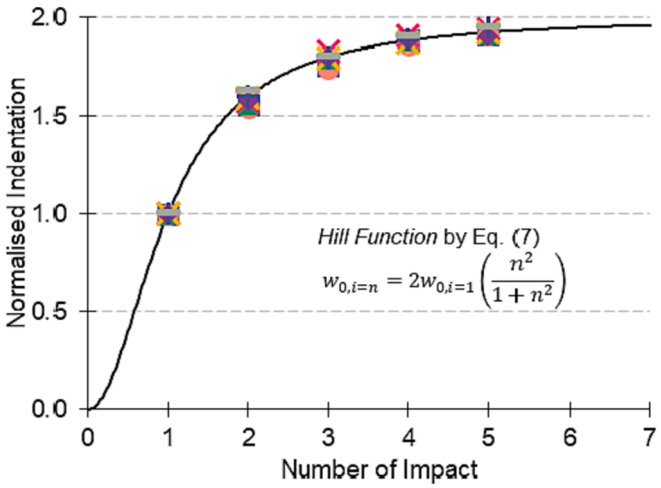

Fig. 7. Relationship between the permanent indentation and the number of impacts approximated by *Hill Function* in the form of Eq. (7).

panel following (many) repeated strikes at the same position is approximately twice the amount of initial indentation generated by the first impact.

Expressions presented in this section are based on multiple impact by ice of the same size and velocity of impact. In a real hailstorm, the size of hail varies. Thus, the analytical model for predicting cumulative indentation is developed further in the next section to incorporate the size distribution of hail in a real storm.

3. Modelling the natural variability of hail induced damage

3.1. Hailstone particle size distribution model (PSD)

In many studies that have been reported in the literature on the damaging potential of hail, the considered scenarios were typically based on impact by ice of a pre-defined size [21,24,63]. The more recent investigation on multiple strikes by hail as presented in the previous section was also dealing with ice impactors of the same size in the considered impact sequence. This section presents results from an investigation conducted by the authors on the particle size distribution (PSD) of hail to realistically represent the behaviour of a real hailstorm. The PSD of hail as presented herein is expressed as a function of the (targeted) area of the panel and the maximum hailstone diameter based on findings from monitoring studies in the field of meteorology [64,65]. Amongst the mathematical models that have been employed for modelling the PSD of hail, the two most commonly adopted models are the exponential distribution function [64,65] and the gamma distribution function [66,67]. Gamma PSD functions are used when modelling hail hazard at the ground level. This type of function featuring a highly left-skewed distribution considering the effects of melting and sublimation of the smaller hailstones which is likely to have occurred at the time of observation. In this study, the hail size distribution was instead modelled at the surface of the targeted cladding panel. The PSD is therefore expected to closely resemble conditions aloft in the cloud which is better represented by the exponential distribution function [65]. Thus, the governing equation employed for the modelling was of the form shown by Eq. (8).

$$n(D) = N_0 \exp(-\lambda D) \tag{8}$$

where $n(D)$ is the particle size distribution of hailstones within an air parcel expressed in terms of the number the hailstones in the diameter interval of (D, $D + dD$) per volume of air. Parameters N_0 and λ are constants for calibration against results from field observations.

PSD of the form used in Eq. (8) can be adapted for defining number density (ρ_N) and hit rate (Hr) as shown by Eqs. (9) and (10), respectively.

$$\rho_N = \int n(D)dD \tag{9}$$

$$Hr = \int v_T(D)n(D)dD \tag{10}$$

where $v_T(D)$ as defined by Eq. (11).is the terminal velocity of a fallen hailstone expressed as function of its size (diameter).

$$v_T(D) = \sqrt{\frac{4\rho_h g D}{3\rho_a C_d}} = \sqrt{\frac{4\rho_h g}{3\rho_a C_d}}\sqrt{D} = v_0 D^{\frac{1}{2}} \tag{11}$$

where, ρ_h is density of hail, ρ_a is density of air, and C_d is drag coefficient, and v_0 becomes a numerical constant consequently.

Integrals in Eq. (9), and in Eq. (10), become solvable should their limits be established. These lower and upper limits were taken as the smallest and largest diameter of hail (D_S and D_L), respectively. Substituting expressions for PSD as defined by Eq. (8) and $v_T(D)$ as defined by Eq. (11) into Eqs. (9) and (10) gives Eqs. (12) and (13) for determining the value of ρ_N and Hr, respectively.

$$\rho_N = \int_{D_S}^{D_L} n(D)dD = N_0\lambda^{-1}\left(e^{-\lambda D_S} - e^{-\lambda D_L}\right) \tag{12}$$

$$Hr = \int_{D_S}^{D_L} v_T(D)n(D)dD = v_0 N_0 \lambda^{-1.5}[\gamma(1.5, \lambda D_S) - \gamma(1.5, \lambda D_L)] \tag{13}$$

where γ is the lower incomplete gamma function.

Meanwhile, the average size of hailstones as observed at the ground level (D_A) can be calculated using Eq. (14).

$$D_A = \frac{1}{Hr}\int_{D_S}^{D_L} D v_T(D)n(D)dD = \frac{v_0 N_0}{Hr}\lambda^{-2.5}[\gamma(2.5, \lambda D_S) - \gamma(2.5, \lambda D_L)] \tag{14}$$

Substituting Eq. (13) into Eq. (14) would allow the value of λ to be determined as function of D_L, D_S, D_A using Eq. (15). Eq. (13) can also be rearranged into Eq. (16) which has N_0 to be the subject of the expression.

$$\lambda = \frac{1}{D_A}\frac{\gamma(2.5, \lambda D_S) - \gamma(2.5, \lambda D_L)}{\gamma(1.5, \lambda D_S) - \gamma(1.5, \lambda D_L)} \tag{15}$$

$$N_0 = \frac{Hr}{v_0}\frac{\lambda^{1.5}}{\gamma(1.5, \lambda D_S) - \gamma(1.5, \lambda D_L)} \tag{16}$$

Note, Eqs. (15) and (16) for determining the value of λ and N_0 could be simplified (reduced) into a form where D_L is the sole variable. The simplification made use of correlations of D_L with other parameters namely D_S, D_A, and Hr. Such correlations became available through analysis of results obtained from field measurements [65]. The predictive expressions of Eqs. (17a) – (17c) were subsequently derived by making use of these correlations.

$$D_S = 1.004 D_L^{0.542} \tag{17a}$$

$$D_A = 1.449 D_L^{0.649} \tag{17b}$$

$$Hr = 153.403 D_L^{-1.087} \tag{17c}$$

where, D_s and D_L are in the unit of mm, and Hr is in the unit of $\text{min}^{-1}\text{m}^{-2}$.

A list of values for λ and N_0 for substitution into Eq. (8) for a range of values of D_L is presented in Table 2.

The predictive expressions listed above are based on the assumption of stationarity in the size distribution of hailstones in a storm. A more rigorous model incorporating non-stationarity is to specify a gradual change in the maximum size of hailstone (D_L) as a function of time (t_h) during a storm. In a World Meteorological Organisation (WMO) manual, a parabolic function of the form shown by Eq. (18) is recommended to

Table 2
Calculated values of N_0 and λ for some predefined (and constant) values of D_L.

D_L(mm)	N_0	λ
20	0.1683	0.1873
30	0.0869	0.1562
40	0.0481	0.1328
50	0.0292	0.1158
60	0.0191	0.1030

express D_L as function of t_h.

$$D_L(t_h) = 5 + \frac{4}{T_h}(D_L - 5)t_h - \frac{4}{T_h^2}(D_L - 5)t_h^2 \tag{18}$$

where T_h is the total duration of the hailstorm (in min) which can be estimated using Eq. (19); D_L is in the unit of mm.

$$T_h = 5.756 + 0.253D_L \tag{19}$$

where T_h is expressed in minutes, and D_L in mm. Expression characterising the time-dependent behaviour of D_L can be substituted into Eqs. (17a) – (17c) for estimating the time-dependent behaviour of D_S, D_A, and Hr.

In summary, the size distribution of hail in a random hailstorm can be estimated by the combined use of Eqs. (17a)– (17c), and optionally (18) and (19), when the expected maximum hailstone diameter (D_L) is given to define the considered storm scenario. Table 2 lists the numerical values of parameters: N_0 and λ in Eq. (8) for some assumed values of D_L. Note, N_0 and λ would also become time-dependent as defined by Eq. (18) (as opposed to being constant with time as assumed in Table 2). The size distribution model as presented in the above is critical to the accurate estimation of hail damage caused to skylights, roofing panels, claddings and automobile components. Eq. (20) can be employed for calculating the total number of hailstones expected to strike a panel of one square metre (N_t) in a storm [65].

$$N_t = 73616D_L^{-0.917} \tag{20}$$

where N_t is in the unit of m^{-2}. The accuracy of the PSD model of hail has been validated by field measurements from meteorological studies [64,65].

For a given surface of a targeted cladding which is exposed to hail, the total expected number of strikes by hailstones in each size domain can be calculated as the product of the value of N_t calculated using Eq. (8) and the exposed area. Consider a hailstorm which is characterised by D_L of 50 mm, the distribution of hailstones impacting the targeted panel of planar dimensions: 900 mm × 900 mm in the storm event is presented in Fig. 8. Estimates by two models are presented in the figure: (i) model assuming stationary behaviour of D_L during the storm and (ii) model taking into account non-stationarity in the behaviour of D_L during the storm as defined by Eq. (18). The second model incorporating a time-dependent D_L is expected to provide a more realistic, and less conservative, estimation of the number of strikes by hail, as the distribution of hail size tends to be more skewed towards smaller size domain.

3.2. Distribution of permanent indentation

Hail induced damage on aluminium alloy cladding is typically manifested in the form of permanent indentation into the metal surface. The amount of permanent indentation generated by the strike of a hailstone on the aluminium panel can be correlated with the amount of energy absorbed as reflected in Eqs. (3) and (7). The amount of absorbed energy is in turn dependent on the size of hail.

Eq. (8) for defining the size distribution of hail can be expressed in the form of probabilistic density function (PDF) as shown by Eq. (21).

$$f(D) = \lambda \exp(-\lambda D) \tag{21}$$

It can be shown that the PDF of the size of hail can be transformed into Eq. (22) for defining the PDF of permanent indentation caused to the aluminium panel.

$$f\left(w_{0,i=n}\right) = f(D) \times \frac{dD}{dw_{0,i=n}} \tag{22}$$

where $\frac{dD}{dw_{0,i=n}}$ is the derivative of the diameter of the ice impactor with respect to the permanent indentation (and can be found by rearranging Eqs. (3) and (7) followed by differentiation).

Eq. (22) enables the distribution of permanent indentation on a targeted panel to be predicted taking into account the natural variability of the size of hail in a storm event. The prediction was based on an incident impact velocity of 40 m/s, which is a value that exhibits minimal variation among various sizes of hail after factoring in the local horizontal wind acceleration [24]. The PDFs of the permanent indentation on aluminium alloy panels of two different dimensions: (i) 900 mm × 900 mm × 3 mm thick and (ii) 900 mm × 900 mm × 4 mm thick as calculated using Eq. (22) are presented in Fig. 9a based on exposing the panels to a single hailstorm event with maximum hail size of 50 mm (i.e., $n = 1$, $D_L = 50mm$). The PDFs presented in Fig. 9b are predictions of the amount of cumulative permanent indentation caused to a 900 mm × 900 mm × 3 mm thick panel following a number of storm events (up to 5) all of which can be characterised by a maximum hail diameter of 50 mm (i.e., $n = 5$, $D_L = 50mm$). The probability of a permanent indentation exceeding a particular threshold is ascertained by computing the area under the probability density curve to the right of the specified threshold value. It is worth noting that the total area beneath each probability density distribution curve shown in Fig. 9 is equal to unity. With increasing number of hailstorm events, the

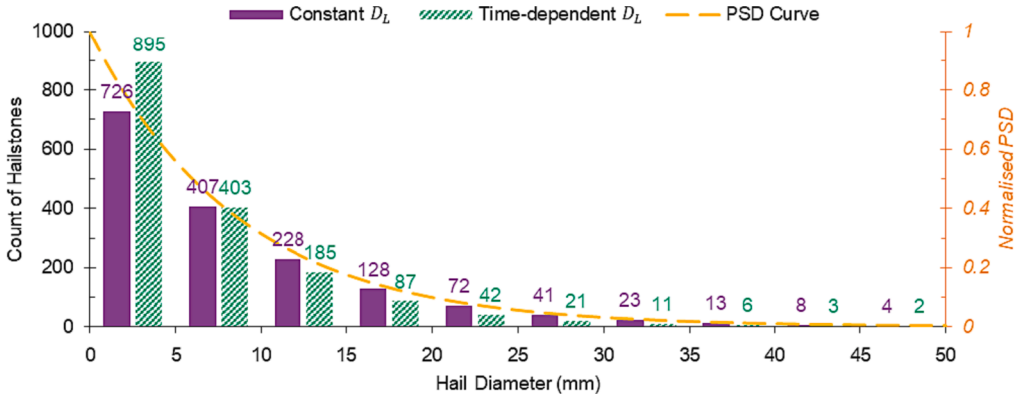

Fig. 8. Distribution of hailstone impacting a cladding panel with planar dimensions of 900 mm × 900 mm in a hailstorm event with an expected maximum diameter of 50 mm.

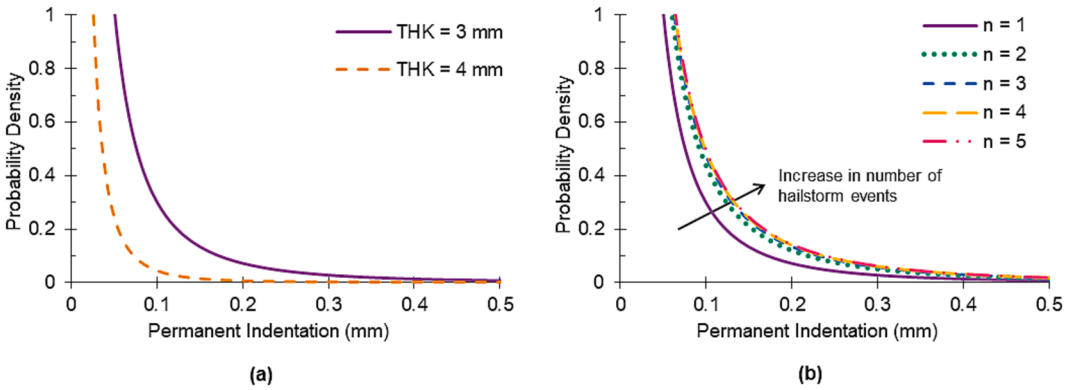

Fig. 9. Probability density functions (PDF) of permanent indentation into an aluminium alloy cladding panel with planar dimensions of 900 mm × 900 mm from hailstorms with maximum hail diameter of 50 mm (a) PDFs of indentation into panels of two different thicknesses in a single storm (b) PDFs of indentation into a 3 mm thick panel following multiple storm events.

probability of having a larger indentation would increase in the manner shown in Fig. 9b. The rate of increase would diminish with increasing number of events in the manner as shown by the probability density curves.

Expressions presented in this section are based on damage caused to the cladding in one hailstorm. The analytical model for predicting cumulative indentation is developed further in the next section to incorporate impact by all hailstorms throughout the service life of the building.

4. Life-cycle analysis methodology and framework

4.1. Overview

Reliability-based models inform us on how a system, or a component, would perform and fail over its service life. In this section, a reliability-based framework is introduced to model the life-cycle performance of aluminium alloy cladding in the context of hailstorm hazards. The parameter for measuring system performance is permanent indentation, $W(t)$. In the life-cycle analysis framework, it is hypothesised that once the cladding panel is installed, damage (indentation) would begin to accumulate when experiencing hailstorms up to the state of failure, or severe deterioration, necessitating intervention. Considering the random nature of hailstorm occurrence, damage accumulation can be modelled as a jump process taking into account interevent time intervals (to be represented in stochastic terms). As damage to the cladding panels (in the form of indentation) accumulates over time, the degree of vulnerability would continue to increase up to the state of failure or replacement.

4.2. Establishment of intervention criteria

In the context of hailstorm hazards, the state of damage is measured by the degree of permanent indentation into the surface of the panel. As the amount of indentation reaches a certain threshold, intervention is warranted. The threshold can be interpreted in various ways. The lower threshold is to do with aesthetic considerations, whereas the upper threshold is associated with protection functionality or structural integrity. For example, the upper threshold is reached when perforations occur leading to ingress of rainwater. The amount of indentation generated by hail impact on cladding panels made of aluminium alloy is typically small compared to the thickness of the panel, evident from Section 2.2 and previous study [50]. Therefore, visible indentation that is discernible to the naked eye which corresponds to aesthetic imperfections was selected as the criterion of necessitating intervention in this section. The lower threshold (refer to W^* as annotated in Fig. 1) is typically not specified in codes of practice but is instead based on practical experience. The visibility of the indentation on a cladding can be controlled by factors such as illumination, colour of the cladding, angle of view, and eyesight distance. Judgement made from experimental observations from testings [68] points to a value of the order of 0.3 mm ~ 0.5 mm as the lower threshold.

4.3. Hazard function

An effective approach of modelling the rate of occurrence of hailstorms, and the damaging potential of a storm event, is through the use of the *marked point process* which is elaborated herein. In a life-cycle analysis, the probability that the indentation on the panel exceeds a pre-defined threshold in a given time span [0, t] can be expressed in the form of Eq. (23).

$$P(T \le t) = F_T(t) = 1 - \bar{F}_T(t) \tag{23}$$

where, $P(T \le t)$ is probability to be determined, $F_T(t)$ is the cumulative damage as function of time and $\bar{F}_T(t)$ is the complementary function (also known as the reliability function).

The hazard function (or hazard rate) which expresses the likelihood of indentation exceeding the pre-defined threshold during the time interval: t to $t+dt$ is defined by Eq. (24) [36].

$$P(exceeding,\ t \le T \le t+dt) = \frac{P(t \le T \le t+dt)}{1 - P(T \le t)} \tag{24}$$

As the time interval dt tends to a very small value (i.e., $dt \to 0$), the nominator in Eq. (24) can be interpreted as the time derivative of function $F_T(t)$ as shown by Eq. (25).

$$P(t \le T \le t+dt) \approx \frac{d}{dt}[F_T(t)] = f_T(t) \tag{25}$$

Expression for the hazard function $h_T(t)$ can be written in the form of Eq. (26), by substituting Eq. (25) into Eq. (24).

$$h_T(t) = \frac{f_T(t)}{1 - F_T(t)} = \frac{f_T(t)}{1 - \int_0^t f_T(t)} \tag{26}$$

4.4. Damage accumulation until intervention

Permanent indentation into an aluminium alloy cladding generated in a hailstorm (known as the "mark" in the *marked point process* model) may be represented by a positive random variable W. The value of W_n represents the amount of indentation caused to the surface of the cladding in the n^{th} hailstorm based on the distribution function: $g_n(w)$. In the context of hail impact on aluminium alloy claddings considered in the current study, $g_n(w)$ shares the same definition as $f(w_{0,i=n})$ as defined by

Eq. (22). At the instance t, the accumulated damage $S(t,n)$ and the remaining capacity $R(t,n)$, can be predicted using Eqs. (27) and (28), respectively.

$$S(t,n) = W_1 + W_2 + \cdots + W_n = \sum_{i=1}^{n} W_i \tag{27}$$

$$R(t,n) = W^* - D(t,n) = W^* - \sum_{i=1}^{n} W_i \tag{28}$$

The amount of cumulative damage and remaining capacity is highly dependent on the passage of time (t) and the number of previously occurred hailstorm events (n).

Assuming that intervention occurs only after a hailstorm event, the probability of intervention (PoI) can be interpreted as the likelihood of a sufficiently large indentation formed at time t, leading to cumulative damage exceeding threshold W^*, as illustrated by the area bounded by W^*, the w-axis and the distribution function $g_n(w)$ as shown in Fig. 1. This time-dependent intervention probability can be found using Eq. (29).

$$PoI(t) = \left(\int_{R(t,n)}^{\infty} g_n(w)dw \right) h_T(t) = \left(\int_{R(t,n)}^{\infty} dG_n(w) \right) h_T(t) \tag{29}$$

The complexity of the computation to solve for Eq. (29) lies in the determination of the lower limit of the integral, $R(t,n)$. While Eq. (28) provides a generic definition of the remaining capacity $R(t,n)$, quantifying W_n would require the preceding remaining capacity that accounts for all the accumulated damages to be known, as shown by Eq. (29).

$$W_n = \int_0^{R(t,n-1)} w dG_n(w) \tag{29}$$

By conditioning the number of hailstorm events (n), Eq. (28) can be rewritten into Eq. (30).

$$R(t,n) = W^* - \sum_{i=1}^{n} \left[\int_0^{R(t,i-1)} w dG_i(w) \right] \tag{30}$$

It is shown by Eq. (30) that the remaining capacity $R(t,n)$ is also dependent on the number of previously occurred hailstorm events which is a random variable. If the probability of having n events by time t, denoted herein as $P(i=n,t)$, the expression for PoI can be rewritten into Eq. (31) in a series format.

$$PoI(t) = \sum_{n=0}^{\infty} \left(\int_{R(t,n)}^{\infty} dG_n(w) \right) h_T(t) P(i=n,t) \tag{31}$$

Estimation from Eq. (31) reflects the instantaneous intervention rate at the current time step. Conversely, the cumulative intervention rate (CIR), evaluated as the definite integral of the instantaneous intervention rate in the time domain [0, t], offers a broader view of the cladding performance over a certain timeframe. The definition of CIR is shown in Eq. (32).

$$CIR(t) = \int_0^t \left[\sum_{n=0}^{\infty} \left(\int_{R(t,n)}^{\infty} dG_n(w) \right) h_T(t) P(i=n,t) \right] d\tau \tag{32}$$

5. Case study

In this section, a case study is presented to illustrate the practical application of the proposed reliability-based life-cycle analysis methodology. The case studies to be presented in this section were based at two locations: the Australian state of Victoria and that of New South Wales. Studies undertaken for these two Australian states were underpinned by the forthcoming analysis (as reported in Section 5.3) revealing how local weather patterns can significantly affect the lifespan of the same cladding product in different geographical locations. In this context, the state of New South Wales in Australia is ranked higher than Victoria in terms of the severity of hail hazards expressed in terms of the frequency of occurrences of hailstorms for given maximum size of hail in the storm. The aim was to illustrate the assessment of the performance of aluminium alloy claddings employing the proposed methodology.

5.1. Occurrence rate of hailstorm events in Australia

The relationship between return period and level of severity of hailstorms is crucial to the application of the hazard function as defined by Eq. (26). The return period refers to the average time intervals between hailstorm events, whereas the level of severity refers to the intensity of hailstorms expressed in terms of the maximum size (diameter) of hail recorded in the event. Hailstorms with higher intensity (larger hailstone size), tend to exhibit longer return periods compared to milder hailstorms. The count of hailstorms in the state of Victoria (1960 ~ 2016) and New South Wales (1900 ~ 2019) for different ranges of maximum diameter of hailstones recorded in these events are listed in Table 3.

The presented information was extracted from the Australian Bureau of Meteorology (BoM) archive of severe hailstorms. Note, hailstones with diameter of less than 20 mm are expected to have melted shortly after hitting the ground. This is a source of error posing challenges in the correct interpretation of data. Thus, small hailstones of diameter in the range: [0, 20) may be disregarded given the minor extent of damage that is associated with strikes by these hailstones. The occurrence of hailstorms characterised by different range of diameter of hail can be modelled effectively using a lognormal distribution with the probability density function in the form of Eq. (33).

$$f(D_L;\mu,\sigma) = \frac{1}{\sigma\sqrt{2\pi}D_L} e^{\left(-\frac{(\ln D_L - \mu)^2}{2\sigma^2} \right)} \tag{33}$$

where, μ and σ are the statistical average and standard deviation describing the distribution curve. The numerical values of μ and σ are 1.063 and 0.4081 for Victoria, and 1.2055 and 0.4159 for New South Wales. Data obtained from BoM along with the fitted lognormal distribution curves for Victoria and New South Wales, respectively, are presented in Fig. 10a and Fig. 10b, respectively, in the form of histograms.

Solving for the integrals in Eq. (33) between the limits: $[D_1, D_2)$ gives estimate for the cumulative probability of having a hailstorm with the largest hail diameter falling in the specified range. The average rate of occurrence (ν) for a given range of size of hail can be calculated by taking the product of the cumulative probability associated with each range of hail diameter and the corresponding annual rate of occurrence. The annual rate of occurrence is determined by dividing the total number of recorded hailstorm events over the number of years of observation. The calculated average rates of occurrence for each range of hail diameter (greater than 20 mm) are listed in Table 4.

Table 3
Number of hailstorms in Victoria (1960 ~ 2016) and New South Wales (1900 ~ 2019) for different hail diameter ranges.

Hail diameter range (mm) *Lower bound included*	Number of hailstorm events	
	Victoria (VIC) 1960 ~ 2016	New South Wales (NSW) 1900 ~ 2019
0 ~ 10	1	5
10 ~ 20	7	16
20 ~ 30	209	586
30 ~ 40	66	305
40 ~ 50	92	444
50 ~ 60	22	163
> 60	27	172

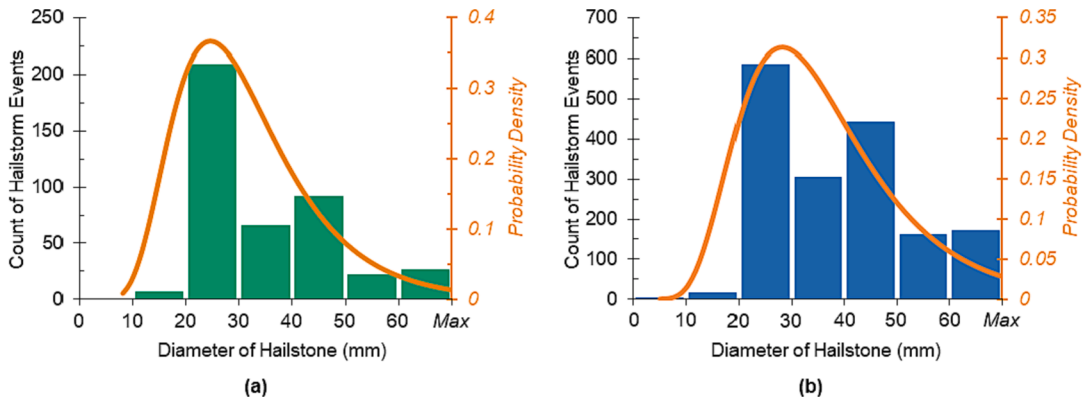

Fig. 10. Distribution of hailstorm events characterised by the maximum recorded hail diameter (a) Victoria (1960 ~ 2016) (b) New South Wales (1900 ~ 2019).

Table 4
Average occurrence rate and return periods of hailstorms in Victoria and New South Wales for different hail diameter ranges.

Hail diameter range (mm) *Lower bound included*	Average occurrence rate ν (per year)	
	Victoria (VIC)	New South Wales (NSW)
20 ~ 30	2.62	4.08
30 ~ 40	1.87	3.80
40 ~ 50	0.92	2.34
50 ~ 60	0.40	1.22
> 60	0.28	1.12

Results presented in Table 4 can be incorporated into the hazard function as defined by Eq. (26) by the use of the Poisson distribution as shown by Eq. (34).

$$h_T(t) = \frac{f_T(t)}{1 - \int_0^t f_T(t)} = \frac{\nu e^{-\nu t}}{1 - (1 - e^{-\nu t})} = \nu \tag{34}$$

5.2. Probability of intervention required for cladding panels

Consider the case of a newly installed aluminium alloy cladding panel located in the state of Victoria, Australia. The panel is made of aluminium alloy of grade 5083-H116. Relevant material properties are listed in Table 1. The average rate of occurrence of hailstorms (characterised by the maximum hailstone diameter) can be estimated by making reference to Table 4. For newly installed claddings which have 100 % of the initial capacity, the threshold for visible permanent indentation to occur can be set at 0.3 mm (i.e., $W^* = 0.3mm$). By these assumptions, the expected service life for the considered panels can be analysed by employing the life-cycle analysis methodology proposed in this paper.

The analysis is initiated at time step $t = 0$ with step size of 1 year. At each step, contributions by every storm event $W_n, n = 1, 2, 3, \cdots$ will have to be considered. The expected extent of damage (indentation) corresponding to each scenario (n) is first estimated using Eqs. (22) and (29), followed by the remaining capacity which is obtained from Eq. (30). The calculated remaining capacity $R(t, n)$ is then substituted into the lower limit of the integral in Eq. (31). The only parameter that remains unknown in Eq. (31) is $P(i = n, t)$. Based on the Poisson distribution shown in Eq. (34), which was adopted to model the hazard function and interarrival time between hailstorm events, the probability of having n hailstorm events by time t can be calculated using Eq. (35).

$$P(i = n, t) = \frac{(\nu t)^n e^{-\nu t}}{n!} \tag{35}$$

The estimated probability of intervention as calculated by the use of Eq. (31) pertains to the intervention rate at the evaluated time step, which is also known as the instantaneous intervention rate. In contrast, the cumulative intervention rate (*CIR*), as illustrated in Eq. (32), provides a more comprehensive perspective on the overall performance of the cladding panel over a specified timeframe. This measurement is obtained by integrating the instantaneous intervention rate over time, which can be utilised in the evaluation of system reliability and the estimation of maintenance, or replacement, intervals. The behaviour of the cladding panel for different intensity levels of hailstorms is well illustrated by the cumulative intervention rate as shown by the graphs in Fig. 11a. The combined probability of intervention, which is calculated by taking the weighted average probability densities as obtained from Eq. (33) for each intensity level is shown in Fig. 11b.

5.3. Factors affecting the performance (sensitivity analysis)

Factors influencing the performance of cladding panels have been investigated. Three key factors that are considered to be critical are: (i) geographical location, (ii) intervention criteria that has been implemented, and (iii) thickness of the cladding panel. It can be inferred from data presented in Table 2 and 3 that cladding panels installed in New South Wales are more susceptible to hail damage than the Victorian counterparts because of a significantly higher rate of occurrence of hailstorms in New South Wales. A higher frequency of hailstorm events necessitates shorter arrival time of intervention. It is shown in Fig. 12a that the expected intervention time for a panel installed in New South Wales is much shorter than in Victoria when the threshold is set at the same level.

Intervention criteria based on visibility of dents can be subject to various factors, such as illumination and colour of the cladding. As depicted in Fig. 12a, increasing the limit of tolerance from 0.3 mm to 0.5 mm can prolong the expected intervention time by approximately 5 and 7 years for New South Wales and Victoria, respectively.

Aluminium alloy claddings that are available in the market were commonly manufactured to a thickness of 3 mm because of considerations of the self-weight of the cladding and cost of construction while complying with strength requirements. Areas that are prone to higher hail hazards, such as cities in the state of New South Wales for example, would warrant cladding panels of greater thickness for improved robustness. Cladding panels with a thickness of 4 mm, though less common, offer an extended service life. It is shown in Fig. 12b that 4 mm thick cladding panels are expected to last nearly three times longer on average compared to 3 mm thick panels with the same intervention criteria.

In summary, the application of the proposed framework of modelling, as demonstrated through case studies in different Australian states, offers a versatile concept and methodology that can be readily transferable to various geographical contexts. When historical records of past hailstorm events and the associated maximum hailstone diameters are accessible for a designated location, Eq. (33) can be employed to determine the average rate of occurrence and return period of hailstorm

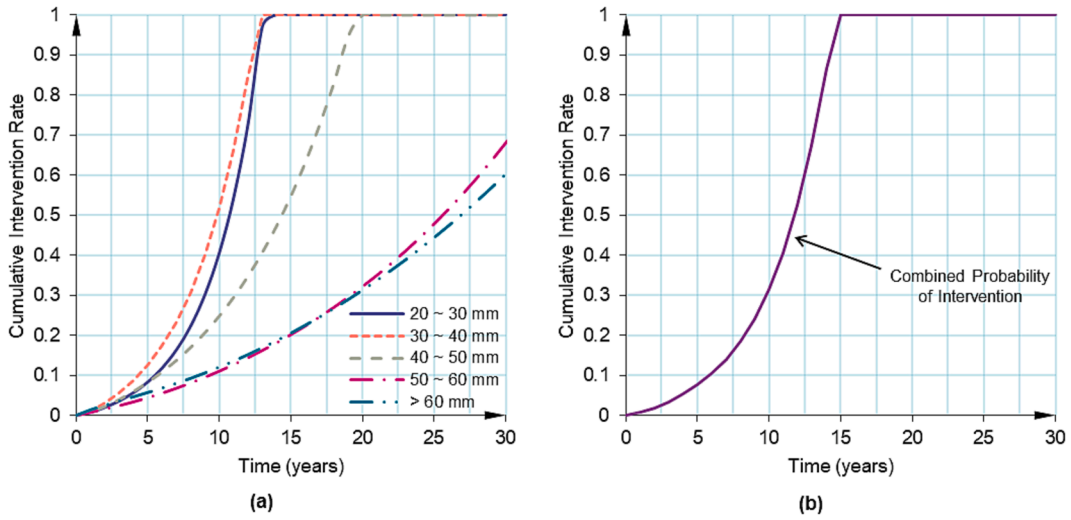

Fig. 11. Cumulative intervention rate by time t of an aluminium cladding panel located in Victoria with a thickness of 3 mm and a maximum allowable indentation of 0.3 mm (a) intervention rate curves of different hailstorm events characterised by the maximum hail diameter (b) combined cumulative intervention rate.

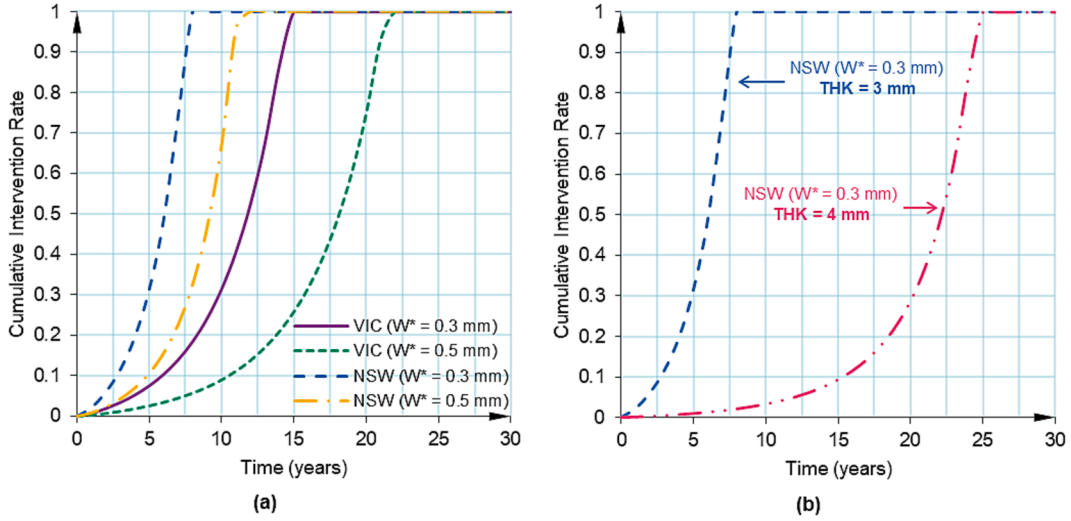

Fig. 12. (a) Effect of geological region and intervention criteria on the cumulative intervention rate (b) effect of panel thickness on the cumulative intervention rate.

events, categorised by their severity. Subsequently, the level of hazard can be found using Eq. (34). The combined use of Eqs. (32) and (35) would then enable the cumulative intervention rate of cladding products to be determined in the region of interests for informing the stakeholders.

6. Conclusion

A life-cycle analysis framework is introduced in this study for evaluating, and predicting, the performance of aluminium alloy claddings to withstand hail hazards. The ability of the presented methodology in providing accurate estimate of the probability of necessary intervention for a projected period has been proven. Through leveraging historical observations from meteorological data (such as that archived by the Australian Bureau of Meteorology), the stochastic characteristics of hailstorm occurrence could be captured. By incorporating the natural variations in the size of hailstones, the precision of damage predictions has been enhanced significantly.

Utilising the probabilistic hail size distribution model as input, the proposed framework demonstrates the capability of estimating the probabilistic distribution of permanent indentation and the resulting damage to claddings following a hailstorm. Experimental observations from 40 gas gun tests have further enhanced the versatility of the framework in evaluating life-cycle performance of panels subjected to multiple hailstorm events.

The practical application of the proposed framework is illustrated through case studies in the Australian states of Victoria and New South Wales. Notably, in regions prone to hailstorms, 3 mm thick aluminium alloy claddings which are commonly used might not perform satisfactorily. A cladding thickness of 4 mm is recommended for improved resilience.

In conclusion, the outcomes of this study provide valuable insights for system reliability evaluation and equip users in the building industry with enhanced decision-making capabilities for improving the long-term performance of aluminium alloy claddings.

CRediT authorship contribution statement

Shuangmin Shi: Methodology, Investigation, Data curation, Formal analysis, Validation, Visualization, Writing – original draft, Writing – review & editing. **Nelson Lam:** Conceptualization, Writing – review & editing, Supervision, Funding acquisition. **Yiwen Cui:** Investigation, Data curation, Formal analysis. **Guoxing Lu:** Conceptualization, Methodology, Resources, Funding acquisition. **Emad Gad:** Conceptualization, Funding acquisition. **Lihai Zhang:** Conceptualization, Methodology, Writing – review & editing, Supervision, Funding acquisition, Project administration.

Declaration of competing interest

The authors declare that they have no known competing financial interests or personal relationships that could have appeared to influence the work reported in this paper.

Data availability

Data will be made available on request.

Acknowledgements

This work is financially supported by the Australian Research Council Linkage Project (ARC LP190100208). Cash and in-kind support by Mr Ian Bennie (General Manager of *Ian Bennie and Associates*) and Mr Suresh Sutrave (Managing Director of *Atlite Skylights*) as Partner Investigators of the linkage project are gratefully acknowledged. The authors are also grateful to Mr Kubendra Rao, Mr Jasman Anwar and Mrs Josie Stokoe for their kind help in the preparation of the test apparatus. The authors wish to thank Dr Shanqing Xu, Mrs Cong Wang and Ms Jia Ming Goh for their generous support during the experiment.

References

[1] Minor JE. Windborne debris and the building envelope. J Wind Eng Ind Aerodyn 1994;53(1–2):207–27.
[2] Sparks PR, Schiff S, Reinhold T. Wind damage to envelopes of houses and consequent insurance losses. J Wind Eng Ind Aerodyn 1994;53(1–2):145–55.
[3] Sparks P. Wind speeds in tropical cyclones and associated insurance losses. J Wind Eng Ind Aerodyn 2003;91(12–15):1731–51.
[4] Ali M, et al. Simple hand calculation method for estimating deflection generated by the low velocity impact of a solid object. Aust J Struct Eng 2014;15(3):243–59.
[5] Yang Y, Lam N, Zhang L. Evaluation of simplified methods of estimating beam responses to impact. Int J Struct Stab Dyn 2012;12(03):1250016.
[6] Yang Y, Lam N, Zhang L. Estimation of response of plate structure subject to low velocitiy impact by a solid object. Int J Struct Stab Dyn 2012;12(06):1250053.
[7] Yang Y, et al. Simplified analysis of low velocity impact actions on shallow domes. Int J Appl Mech 2013;5(02):1350013.
[8] Yong, A.C., N.T. Lam, and S.J. Menegon, Collision Actions on Structures. 2022: CRC Press.
[9] Yang Y, et al. An innovative procedure for estimating contact force during impact. Int J Appl Mech 2014;6(06):1450079.
[10] Sun J, et al. Contact forces generated by fallen debris. Struct Eng Mech 2014;50(5):589–603.
[11] Sun J, et al. Computer simulation of contact forces generated by impact. Int J Struct Stab Dyn 2017;17(01):1750005.
[12] Shi S, et al. Indentation into an aluminium panel by the impact of a rigid spherical object. Thin-Walled Struct 2022;180:109935.
[13] Herbin A, Barbato M. Fragility curves for building envelope components subject to windborne debris impact. J Wind Eng Ind Aerodyn 2012;107:285–98.
[14] Alphonso T, Barbato M. Experimental fragility curves for aluminum storm panels subject to windborne debris impact. J Wind Eng Ind Aerodyn 2014;134:44–55.
[15] Chen W, Hao H, Du H. Failure analysis of corrugated panel subjected to windborne debris impacts. Eng Fail Anal 2014;44:229–49.
[16] Perera S, et al. Deterministic solutions for contact force generated by impact of windborne debris. Int J Impact Eng 2016;91:126–41.
[17] Pathirana M, et al. Damage modelling of aluminium panels impacted by windborne debris. J Wind Eng Ind Aerodyn 2017;165:1–12.
[18] Cui Y, et al. Flexural Strains in a Toughened Glass Panel generated by Impact of an Ice Sphere. Int J Solids Struct 2023;281:112438.
[19] Cui Y, et al. Deterministic failure prediction of toughened glass when impacted by ice. Int J Impact Eng 2024;185:104833.
[20] Chen S, et al. Experiments on an ice ball impacting onto a rigid target. Int J Impact Eng 2022;167:104281.
[21] Kim H, Welch DA, Kedward KT. Experimental investigation of high velocity ice impacts on woven carbon/epoxy composite panels. Compos A Appl Sci Manuf 2003;34(1):25–41.
[22] Sun J, et al. Contact forces generated by hailstone impact. Int J Impact Eng 2015;84:145–58.
[23] Sun J, et al. A note on Hunt and Crossley model with generalized visco-elastic damping. Int J Impact Eng 2018;121:151–6.
[24] Shi S, et al. An analytical approach for modelling contact forcing function of hailstone impact. Int J Solids Struct 2023;269:112214.
[25] Carney KS, et al. A phenomenological high strain rate model with failure for ice. Int J Solids Struct 2006;43(25–26):7820–39.
[26] Pernas-Sánchez J, et al. Numerical modeling of ice behavior under high velocity impacts. Int J Solids Struct 2012;49(14):1919–27.
[27] Tippmann JD, Kim H, Rhymer JD. Experimentally validated strain rate dependent material model for spherical ice impact simulation. Int J Impact Eng 2013;57:43–54.
[28] Liu K, Li P, Wang Z. A rate-sensitive and pressure-dependent failure criterion for hail ice. Int J Impact Eng 2022;168:104291.
[29] Perera S, et al. Probabilistic modelling of forces of hail. Nat Hazards 2018;91(1):133–53.
[30] Pathirana M, et al. Risks of failure of annealed glass panels subject to point contact actions. Int J Solids Struct 2017;129:177–94.
[31] Pathirana M, et al. Probabilistic modelling of Hertzian fracture of glass by flying objects impact in bad weather. Int J Impact Eng 2018;118:11–23.
[32] Yang W, et al. Time-dependent structural reliability under nonstationary and non-Gaussian processes. Struct Saf 2023;100:102286.
[33] Feng D-C, et al. Time-dependent reliability-based redundancy assessment of deteriorated RC structures against progressive collapse considering corrosion effect. Struct Saf 2021;89:102061.
[34] Li Q, Wang C, Ellingwood BR. Time-dependent reliability of aging structures in the presence of non-stationary loads and degradation. Struct Saf 2015;52:132–41.
[35] Jia G, Gardoni P. State-dependent stochastic models: A general stochastic framework for modeling deteriorating engineering systems considering multiple deterioration processes and their interactions. Struct Saf 2018;72:99–110.
[36] Melchers, R.E. and A.T. Beck, Structural reliability analysis and prediction. 2018: John wiley & sons.
[37] Li, C.-Q. and W. Yang, Time-dependent reliability theory and its applications. 2022: Elsevier.
[38] Sanchez-Silva M, Klutke G-A, Rosowsky DV. Life-cycle performance of structures subject to multiple deterioration mechanisms. Struct Saf 2011;33(3):206–17.
[39] Stewart MG, Rosowsky DV. Time-dependent reliability of deteriorating reinforced concrete bridge decks. Struct Saf 1998;20(1):91–109.
[40] Vu KAT, Stewart MG. Structural reliability of concrete bridges including improved chloride-induced corrosion models. Struct Saf 2000;22(4):313–33.
[41] Sun D, et al. Reliability assessment of concrete under external sulfate attack. Case Stud Constr Mater 2021;15:e00690.
[42] Chen S, et al. Life-cycle modelling of concrete cracking and reinforcement corrosion in concrete bridges: a case study. Eng Struct 2021;237:112143.
[43] Herath N, et al. A reliability-based framework for damage accumulation due to multiple earthquakes: a case study on bridges. Infrastructures 2023;8(6):106.
[44] Cheng C, Zhang L, Thompson RG. Disaster waste clean-up system performance subject to time-dependent disaster waste accumulation. Nat Hazards 2018;91(2):717–34.
[45] Cheng C, Zhang L, Thompson RG. Reliability analysis of road networks in disaster waste management. Waste Manag 2019;84:383–93.
[46] Karyagina M, Wong W, Vlacic L. Life cycle cost modelling using marked point processes. Reliab Eng Syst Saf 1998;59(3):291–8.
[47] Kumar R, Cline DB, Gardoni P. A stochastic framework to model deterioration in engineering systems. Struct Saf 2015;53:36–43.
[48] Biondini F, Frangopol DM. Life-cycle performance of deteriorating structural systems under uncertainty. J Struct Eng 2016;142(9):F4016001.
[49] Sánchez-Silva M, et al. Maintenance and operation of infrastructure systems. J Struct Eng 2016;142(9):F4016004.
[50] Shi S, et al. Indentation modelling of aluminium cladding panels subjected to hailstone impact. Int J Impact Eng 2023;179:104638.
[51] Jones N. Slamming damage. J Ship Res 1973;17(02):80–6.
[52] Shen, W.Q. and N. Jones, The pseudo-shakedown of beams and plates when subjected to repeated dynamic loads. 1992.
[53] Jones N. Pseudo-shakedown phenomenon for the mass impact loading of plating. Int J Impact Eng 2014;65:33–9.
[54] Huang Z, Chen Q, Zhang W. Pseudo-shakedown in the collision mechanics of ships. Int J Impact Eng 2000;24(1):19–31.
[55] Cai W, Zhu L, Qian X. Dynamic responses of steel plates under repeated ice impacts. Int J Impact Eng 2022;162:104129.
[56] Hill AV. The possible effects of the aggregation of the molecules of haemoglobin on its dissociation curves. J Physiol 1910;40:4–7.
[57] Sun D, et al. Deformation behaviour of concrete materials under the sulfate attack. Constr Build Mater 2019;210:232–41.
[58] Sun D, et al. Degradation of concrete in marine environment under coupled chloride and sulfate attack: a numerical and experimental study. Case Stud Constr Mater 2022;17:e01218.
[59] Ren J, Zhang L, San Nicolas R. Degradation process of alkali-activated slag/fly ash and Portland cement-based pastes exposed to phosphoric acid. Constr Build Mater 2020;232:117209.

[60] Ren J, Zhang L, San Nicolas R. Degradation of alkali-activated slag and fly ash mortars under different aggressive acid conditions. J Mater Civ Eng 2021;33(7):04021140.
[61] Zhang L, et al. A fully coupled poroelastic reactive-transport model of cartilage. Mol Cell Biomech 2008;5(2):133.
[62] Zhang L, et al. Integrated model of IGF-I mediated biosynthesis in a deformed articular cartilage. J Eng Mech 2009;135(5):439–49.
[63] Kim H, Kedward KT. Modeling hail ice impacts and predicting impact damage initiation in composite structures. AIAA J 2000;38(7):1278–88.
[64] Field PR, et al. Normalized hail particle size distributions from the T-28 storm-penetrating aircraft. J Appl Meteorol Climatol 2019;58(2):231–45.
[65] Grieser J, Hill M. How to express hail intensity—modeling the hailstone size distribution. J Appl Meteorol Climatol 2019;58(10):2329–45.
[66] Milbrandt J, Yau M. A multimoment bulk microphysics parameterization. Part I: analysis of the role of the spectral shape parameter. J Atmos Sci 2005;62(9):3051–64.
[67] Loftus A, Cotton W, Carrió G. A triple-moment hail bulk microphysics scheme. Part I: description and initial evaluation. Atmos Res 2014;149:35–57.
[68] Bennie, I., Advice sought from personal communication in 2021 with Ian Bennie of Ian Bennie & Associates which is the National Association of Testing Authorities (NATA) sole accredited testing laboratory in Australia. 2021.